THE JOURNAL OF PHYSICAL CHEMISTRY C

Article

pubs.acs.org/JPCC

Puckered Arsenene: A Promising Room-Temperature Thermoelectric Material from First-Principles Prediction

Yajing Sun,[†] Dong Wang,*[,†] and Zhigang Shuai[†,‡,§]

[†]MOE Key Laboratory of Organic OptoElectronics and Molecular Engineering, Department of Chemistry, Tsinghua University, Beijing 100084, People's Republic of China

[‡]Key Laboratory of Organic Solids, Beijing National Laboratory for Molecular Science (BNLMS), Institute of Chemistry, Chinese Academy of Sciences, Beijing 100190, People's Republic of China

[§]Collaborative Innovation Center of Chemistry for Energy Materials, Xiamen University, Xiamen 351005, People's Republic of China

Supporting Information

ABSTRACT: Monolayer arsenic is a newly emerging two-dimensional material in the VA group similar to its isologue, phosphorene. On the basis of first-principles calculations and Boltzmann transport theory, we investigated the electrical, thermal, and thermoelectric transport properties for two forms of monolayer arsenic, arsenene, featuring puckered and buckled structures, respectively. The two kinds of arsenene are both indirect band gap semiconductors possessing moderate to high charge carrier mobilities falling in the range 40−800 $cm^2\ V^{-1}\ s^{-1}$. The puckered arsenene exhibits relatively low and anisotropic lattice thermal conductivities, with 9.6 $W\ m^{-1}\ K^{-1}$ in the armchair and 30.7 $W\ m^{-1}\ K^{-1}$ in the zigzag direction. More significantly, its preferential thermal transport direction is orthogonal to the electrical transport direction, which enhances the thermoelectric figure of merit in the armchair direction to 0.7 for p-doping and 1.6 for n-doping at room temperature.

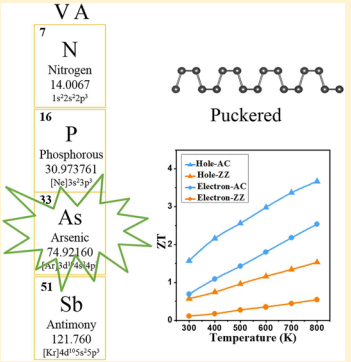

1. INTRODUCTION

In the past decades, researchers have been in the pursuit of highly efficient and earth-abundant thermoelectric materials. The efficiency of thermoelectric materials is determined by its figure of merit, $ZT = S^2(\sigma/\kappa)T$, where S is the Seebeck coefficient, σ is the electrical conductivity, κ is the thermal conductivity, and T is the absolute temperature. As we know, the current state-of-the-art thermoelectric materials are made exclusively from V−VI group elements such as Bi_2Te_3, and IV−VI group compounds such as PbTe and SnSe, which all share a layered crystal structure and possess an intrinsically low thermal conductivity. Moreover, these laminar compounds are readily exfoliated to monolayers or few-layers, and theoretical predictions highlight significant enhancement of figure of merit in Bi_2Te_3 and SnSe nanosheets due to the quantum confinement effect.[1−4] The negative correlation between σ and κ has been demonstrated in SnS_2 sheets, with σ increasing whereas κ decreasing with the decreased thickness of SnS_2.[5] Recently, newly fabricated few-layer phosphorus has been investigated for potential thermoelectric applications.[6,7] It exhibits highly anisotropic electrical,[8,9] optical,[10,11] and thermoelectric responses.[12−14] However, phosphorus is lightweight, exhibiting relatively high thermal conductivity. In contrast, the group VA element, arsenic, which is within the same period as selenium, is much heavier than phosphorus, so it is featured with softer vibrational modes and stronger anharmonicity. Gray arsenic is one of the most stable allotropes of arsenic with a buckled layered structure. The orthorhombic phase (puckered) of arsenic similar to black phosphorus has also been predicted to be stable in the monolayer.[15−21] In a recent experiment, multilayer arsenene nanoribbions have been synthesized on the InAs substrate.[22]

In this paper, first-principles calculations have been carried out to study the electrical and thermal transport properties of single-layered arsenene with buckled and puckered structures. The results show that arsenene, as an indirect band gap semiconductor, possesses moderate to high mobilities for both electrons and holes, 10^2−10^3 $cm^2\ V^{-1}\ s^{-1}$ in the puckered and 10−10^2 $cm^2\ V^{-1}\ s^{-1}$ in the buckled arsenene, which are, respectively, lower than the theoretical predictions for phosphorene[23] and monolayer MoS_2.[24] At the same time, the puckered arsenene exhibits low thermal conductivities, which makes it a potential candidate for two-dimensional (2D) thermoelectric materials. More significantly, both electrical and thermal transport properties are anisotropic in puckered arsenene, with their preferential conducting directions orthogonal to each other. To be specific, the charge carrier mobility in the armchair (AC) direction is 720 $cm^2\ V^{-1}\ s^{-1}$ for electrons and 261 $cm^2\ V^{-1}\ s^{-1}$ for holes and that in the zigzag (ZZ) direction is 512 $cm^2\ V^{-1}\ s^{-1}$ for electrons and 40 $cm^2\ V^{-1}\ s^{-1}$ for holes. Whereas the lattice thermal conductivity is 9.6 $W\ m^{-1}\ K^{-1}$ in the AC direction, it is lower than 30.7 $W\ m^{-1}\ K^{-1}$ in

Received: June 24, 2017
Revised: August 9, 2017
Published: August 10, 2017

DOI: 10.1021/acs.jpcc.7b06196
J. Phys. Chem. C 2017, 121, 19080−19086

the ZZ direction. At room temperature, the maximum ZT in the AC direction is as high as 1.6 when the puckered arsenene is n-doped and it is 0.7 when p-doped, suggesting that puckered arsenene is a highly efficient room-temperature thermoelectric material.

2. METHODS

2.1. DFT Calculation. The lattice parameters and atomic coordinates were optimized by using the projector augmented wave (PAW) method and the Perdew–Burke–Ernzerhof (PBE) exchange-correlation functional as implemented in VASP5.2,[25−27] until all of the forces were less than 0.005 eV/Å per atom. A 20 Å vacuum slab in the through-plane direction was applied to eliminate the interactions between periodic images. The plane-wave basis cutoff was 600 eV. The band structure was calculated by using the HSE06 hybrid functional based on the optimized structure. The spin–orbit coupling was considered in all of the calculations. The interatomic force constants (IFCs) were obtained using the real-space finite displacement difference method. The space group symmetry properties were used to reduce the computational cost and numerical noises of the force constants. The phonon frequencies and eigenvectors were obtained by diagonalizing the dynamical matrix using the Phonopy package.[28]

2.2. Electrical Transport Property Calculation. The electrical transport properties, including the electrical conductivity σ, the Seebeck coefficient S, and the electronic thermal conductivity κ_e, were calculated by solving the Boltzmann transport equation (BTE) using the BoltzTraP package,[29] in which we have incorporated the relaxation time calculation on the basis of the deformation potential (DP) theory[30] and modified the Fourier expansion scheme to the 2D case. The DP theory has been successfully applied for predicting the mobility of 2D materials.[24,31,32] By shifting the Fermi level, we obtained the electrical transport coefficients as a function of carrier concentration in the rigid band approximation. The effective thickness of monolayer arsenic was taken to be 2.4 and 1.4 Å for puckered and buckled structures, respectively, to convert the conductance to the conductivity. The mobility was calculated by $\mu = \sigma/n$, where n is the carrier concentration and determined by the Fermi–Dirac distribution function. A dense $\mathbf{k}$-mesh of 45 × 45 has been used to get converged results. The relaxation time of charge carriers can be expressed as[33]

$$\frac{1}{\tau(\mathbf{k})} = \sum_{\mathbf{k}'} \frac{2\pi}{\hbar} \frac{k_B T E_1^{\,2}}{C_{ii}} \delta(\varepsilon(\mathbf{k}) - \varepsilon(\mathbf{k}'))\cdot(1 - \cos\theta) \tag{1}$$

where the electron or hole deformation potential constant $E_1 = \Delta\varepsilon_{CBM(VBM)}/(\Delta l/l_0)$ was obtained by a linear fitting of the CBM or VBM energy shift with the lattice deformation (Figure S1), while the elastic constant C_{ii} was obtained by a parabolic fitting of the total energy E with the strain $\Delta l/l_0$ via $(E - E_0)/S_0 = C_{ii}(\Delta l/l_0)^2/2$, where E_0 and S_0 are the total energy and area of the unit cell. The energies of VBM and CBM were calibrated with the vacuum level energy. θ is the scattering angle between the two electronic states $\mathbf{k}$ and $\mathbf{k}'$, and k_B and $\hbar$ are the Boltzmann constant and the reduced Plank constant, respectively.

2.3. Lattice Thermal Conductivity Calculation. The Boltzmann transport equation also describes the steady-state resistance to phonon diffusions in a thermal field, arising from scattering of grain boundaries, lattice defects, and other phonons. If the deviation of the phonon distribution from the equilibrium is small, the BTE can be solved by linearizing the scattering term and introducing a phonon mean lifetime. The solution to the Boltzmann equation gives

$$\kappa_L = \sum_{\lambda}^{3n} \int_{\mathbf{q}} v_\lambda^{\,2}(\mathbf{q}) c_\lambda(\mathbf{q}) \tau_\lambda(\mathbf{q})\, d\mathbf{q} \tag{2}$$

where $v_\lambda(\mathbf{q}) = \partial\omega_\lambda(\mathbf{q})/\partial\mathbf{q}$ is the phonon group velocity and $c_\lambda(\mathbf{q}) = (k_B/V)x^2e^x/(e^x - 1)^2$ is the mode-specific heat capacity with $x = \hbar\omega_\lambda(\mathbf{q})/k_BT$.[34] In the Callaway model, the resistive Umklapp phonon–phonon scattering rate can be expressed as[35]

$$\tau_{\lambda,U}^{\,-1}(\mathbf{q}) = \hbar\gamma_\lambda^{\,2}(\mathbf{q})\omega_\lambda^{\,2}(\mathbf{q})T e^{-\Theta_\lambda/3T}/[\bar{M}\Theta_\lambda v_\lambda^{\,2}(\mathbf{q})] \tag{3}$$

where $\bar{M}$ is the average atomic mass and $e^{-\Theta_\lambda/3T}$ controls the onset of resistive Umklapp scattering for each phonon mode through the mode-specific Debye temperature Θ_λ. The Callaway model has been successfully applied to predict the lattice thermal conductivity of many low-dimensional materials.[36,37] The strength of the phonon–phonon scattering for each phonon branch λ is controlled by the Grüneisen constant, which is defined as

$$\gamma_\lambda = -[A/\omega_\lambda(\mathbf{q})][d\omega_\lambda(\mathbf{q})/dA] \tag{4}$$

with A being the area of the supercell. On the basis of DFPT force constant calculations for the arsenene supercell with different cell areas, we can derive the Grüneisen parameters of all phonon modes.

3. RESULTS AND DISCUSSION

Arsenic has various allotropes. In this paper, we chose two monolayer forms, featuring puckered and buckled structures, respectively, to investigate their thermal, electrical, and thermoelectric properties. The monolayer of the most abundant and stable gray arsenic in nature is of the buckled structure, with two arsenic atoms in its unit cell. The other monolayer form is of puckered structure with a rectangular unit cell and four atoms in it, similar to black phosphorene. The geometric structure of monolayer arsenene is presented in Figure 1. Each arsenic atom is covalently bonded to its neighboring arsenic atoms, forming a buckled or puckered 2D honeycomb structure. The optimized lattice parameters and

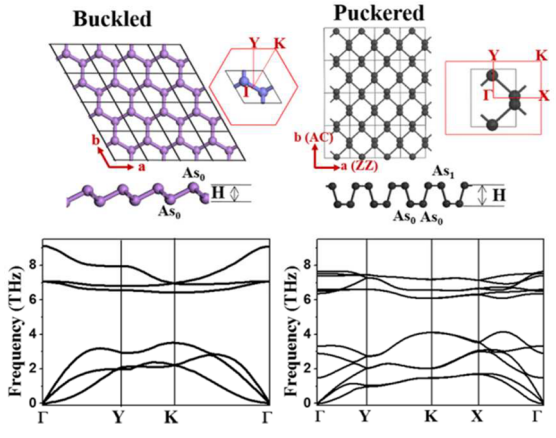

Figure 1. Geometric structures and phonon dispersions of buckled and puckered arsenene.

DOI: 10.1021/acs.jpcc.7b06196
J. Phys. Chem. C 2017, 121, 19080−19086

Table 1. Structural Parameters of Puckered and Buckled Arsenene[a]

	a (Å)	b (Å)	L(As0−As0) (Å)	L(As0−As1) (Å)	H (Å)	∠(As000)	∠(As010)
buckled	3.613	3.613		2.510	1.397		92.05
	3.607[b]	3.607[b]		2.453−2.503[b]			92.22[b]
puckered	3.686	4.777	2.509	2.497	2.401	94.51	100.7
	3.68−3.81[b]	4.75−4.77[b]	2.31−2.50[b]	2.43−2.49[b]		94.64[b]	100.8[b]

[a]a and b are the lattice parameters of the unit cell; L(As0−As0) and L(As0−As1) are the bond length labeled in Figure 1; H is the thickness of monolayer arsenene, referring to the height difference between the top-layer and bottom-layer arsenic atoms; ∠As is the angle. [b]These data are taken from other works.[19,20]

bond lengths were listed in Table 1. They are consistent with those obtained by other researchers.[19,20]

3.1. Electronic Structure and Charge Transport Properties. As mentioned before, the lattice parameters and atomic positions are both optimized by the density functional theory with the Perdew, Burke, and Ernzerhof (PBE) functional. Since the PBE functional usually underestimates the band gap, we further calculate the band structure of arsenene with the HSE06 hybrid functional, which incorporates 20% exact Hartree−Fock exchange interaction. The electronic band structures of puckered and buckled arsenene are shown in Figure 2. Different from their bulk counterparts, both forms of arsenene are indirect band gap semiconductors. The buckled structure exhibits an indirect band gap from the Γ-point to the M-point (the midpoint in the Γ−Y direction) of 2.07 eV. From the projected density of states (PDOS) analysis, its valence band maximum (VBM) is composed mainly of in-plane p orbitals (p_x and p_y) of arsenic atoms, while the conduction band minimum (CBM) consists mainly of out-of-plane p_z orbitals. The electron density distributions at the CBM and VBM of both buckled and puckered arsenene are shown in Figure S2. The puckered structure is also an indirect band gap semiconductor with a band gap of 1.36 eV. Its VBM is located at a point along the Γ−Y high symmetry line with the energy almost degenerate to the Γ point, while the CBM is located at the Γ-point. The band dispersion around the Γ-point is highly anisotropic: both the valence and conduction bands are significantly dispersive along the AC (Γ−Y) direction but are nearly flat along the ZZ (Γ−X) direction. Accordingly, the effective mass of charge carriers in puckered arsenene ($0.37m_e$ vs $0.12m_e$ for electrons and $0.45m_e$ vs $0.05m_e$ for holes along the ZZ and AC directions, respectively) and its mobility (512 $cm^2\ V^{-1}\ s^{-1}$ vs 720 $cm^2\ V^{-1}\ s^{-1}$ for electrons and 40 $cm^2\ V^{-1}\ s^{-1}$ vs 261 $cm^2\ V^{-1}\ s^{-1}$ for holes at the room temperature along the ZZ and AC directions, respectively) are highly anisotropic. The deformation potentials and elastic constants, which account for the strength of acoustic phonon scatterings, are also anisotropic in puckered arsenene, as shown in Table 2.

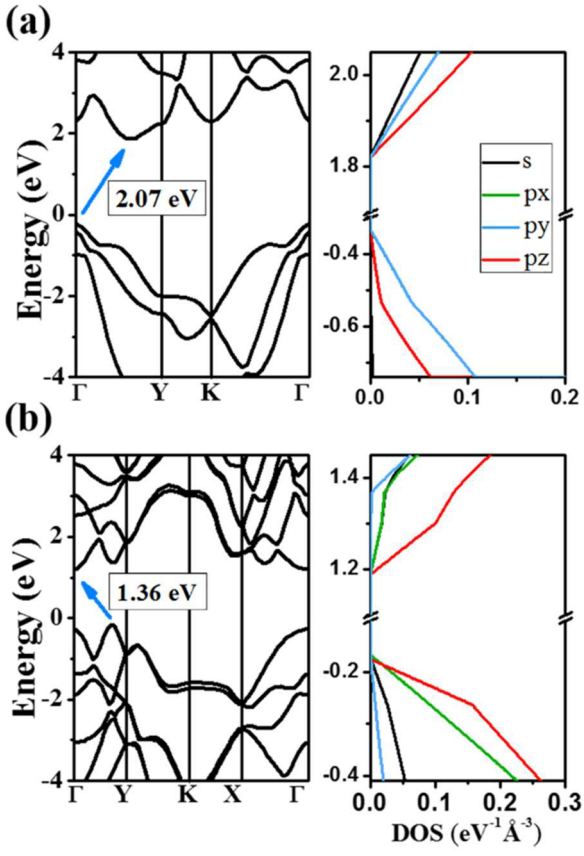

Figure 2. Band structures and projected density of states (DOS) of buckled (a) and puckered (b) arsenene. Both are indirect band gap semiconductors with band gaps of 2.07 and 1.36 eV, respectively.

Table 2. Deformation Potential Constants E_1, Elastic Constants C_{ii}, and Mobilities μ of Electrons (e) and Holes (h) in Buckled and Puckered Arsenene

		direction	E_1 (eV)	C_{ii} (J m^{-2})	m^*/m_e	μ ($cm^2\ V^{-1}\ s^{-1}$)
buckled	e	a (b)	5.3	58.0	0.36	137
	h	a (b)	3.7	58.0	0.43	64
puckered	e	a (ZZ)	4.4	70.6	0.37	512
		b (AC)	2.2	55.1	0.12	720
	h	a (ZZ)	1.0	70.6	0.45	40
		b (AC)	6.7	55.1	0.05	261

At room temperature (300 K), the electron mobility is 137 $cm^2\ V^{-1}\ s^{-1}$ in the buckled structure and the hole mobility is 64 $cm^2\ V^{-1}\ s^{-1}$ along both crystal axis directions a and b, due to its hexagonal symmetry. Our results are consistent with those reported in previous works, where electron and hole mobilities on the order of 10^2−10^3 were predicted.[17,38,39] Obviously, the electrons are more mobile than the holes in both puckered and buckled arsenene. Meanwhile, the hole mobilities exhibit higher anisotropy than the electron mobilities in puckered arsenene, with that along the AC direction more than 6 times larger than that along the ZZ direction.

3.2. Lattice Thermal Conductivity. The thermal conduction in most semiconductors is mediated primarily by lattice vibrations, namely, phonons. There are several scattering effects that hinder the heat transfer, including the phonon−phonon scattering, the phonon−boundary scattering, and the scattering between phonons and impurities or isotope scattering. We model arsenene as infinite and perfect crystals, where we

DOI: 10.1021/acs.jpcc.7b06196
J. Phys. Chem. C 2017, 121, 19080−19086

consider the phonon−phonon scattering process as the only crucial heat-resistance path. The phonon dispersion relation is shown in Figure 1. Both arsenene structures are thermodynamically stable, as evidenced by the absence of imaginary frequencies. Our long-time first-principles molecular dynamics simulations also confirm that both structures remain stable at a temperature of 300 K. The phonon bands have three acoustic modes, including a longitudinal acoustic (LA) mode and an in-plane transverse acoustic (TA) mode both exhibiting linear dispersions around the Γ point, as well as an out-of-plane flexural mode (ZA) exhibiting quadratic dispersion in the long-wavelength limit, which is a general feature of 2D materials.[40] Since the number of atoms in the puckered structure (four arsenic atoms per unit cell) is twice that in the buckled one, the number of phonon modes is also doubled in the former. The frequency gap between the low-frequency and high-frequency optical branches is about 3 THz in the buckled structure, which is much larger than that in the puckered structure (2 THz). The selection rule of three-phonon scattering processes requires that the total energy and momentum of phonons involved in the scatterings are conserved; therefore, the larger frequency gap in the phonon dispersion plot usually indicates suppressed scattering channels, which in turn gives rise to a longer mean free path of phonons and higher lattice thermal conductivity.

Several theoretical methods have been established to predict the lattice thermal conductivity of low-dimensional materials.[41−44] In this paper, we predict the lattice thermal conductivity of arsenene by solving the phonon BTE in the relaxation time approximation and utilizing the Callaway model[35] to derive the phonon relaxation time. The Callaway model considers the Umklapp three-phonon scattering process. Our results of calculation show that the buckled arsenene possesses a thermal conductivity as high as 61 W m^{-1} K^{-1} at 300 K, which is lower than blue phosphorene of 78 W m^{-1} K^{-1}[45] and higher than antimonene of 15.1 W m^{-1} K^{-1},[46] both featuring the buckled structure. Heat conduction in the puckered arsenene is remarkably anisotropic due to its anisotropic bonding and orthorhombic lattice symmetry. Specifically, the thermal conductivity of the puckered arsenene is 30.7 W m^{-1} K^{-1} along the ZZ direction and 9.6 W m^{-1} K^{-1} along the AC direction at 300 K, lower than that of black phosphorene with the same puckered structure, which is 110 and 36 W m^{-1} K^{-1}, respectively, in the ZZ and AC directions.[45] Such a decrease in the thermal conductivity could be attributed to the heavier elements in arsenene, which tend to lower phonon frequencies and group velocities. Our results of the thermal conductivity agree reasonably with those reported earlier by considering three-phonon scattering processes and calculating third-order interatomic force constants from first-principles. The prediction by Donadio et al. for the puckered arsenene is 30.4 and 7.8 W m^{-1} K^{-1} along the ZZ and AC directions, respectively,[47] and that by Ke et al. is 26.1 and 5.6 W m^{-1} K^{-1} for the puckered structure and 65.4 W m^{-1} K^{-1} for the buckled structure.[18] More recently, Carrete et al. also tackled the thermal conduction in 2D arsenene with the first-principles method, focusing on the correlation between the structural complexity and the thermal conductivity.[21] We noticed that, even with the same calculation method, the results may deviate from each other, probably due to the errors in numerical implementations and the effective thickness of 2D materials employed to convert conductance into conductivity.[48] The effective thickness we applied here is 1.4 Å for the buckled arsenene and 2.4 Å for the puckered arsenene. We used the same values in the calculation of electrical conductivity and electronic thermal conductivity, so the choice of effective thickness would not influence the thermoelectric figure of merit. In Figure 3, we present the lattice thermal conductivity

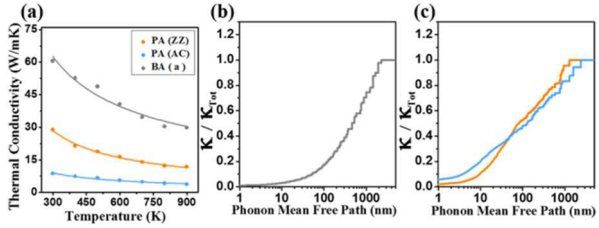

Figure 3. (a) Temperature dependence of lattice thermal conductivities of arsenene with buckled and puckered structures, which follow the T^{-1} law (solid lines). (b and c) Accumulative thermal conductivities κ/κ_{Total} with respect to the phonon mean free path (MFP) in buckled and puckered arsenene, respectively.

of both arsenene structures as a function of the temperature. The thermal conductivities in both directions gradually decrease with the increase of temperature T, following the T^{-1} law, since the phonon relaxation time is inversely proportional to T, as shown in eq 3.

The average phonon relaxation time and mean free path (MFP) of the three acoustic phonon modes in the buckled arsenene (13.8 ps and 46.0 nm) are much larger than those in the puckered arsenene (3.8 ps and 13.1 nm), which is consistent with that inferred from the phonon dispersion plot exhibiting a larger phonon band gap in the buckled arsenene. We also show in Figure 3 the accumulative thermal conductivity as a function of the phonon mean free path. In buckled arsenene, due to the small scattering rate, phonon MFP would be longer than 100 nm. If reducing the size of the material to 100 nm, the lattice thermal conductivity will drop by 90%. The phonon relaxation time and mean free path are shown in Figure S3 as a function of the phonon frequency for all of the phonon modes. We find that the three acoustic phonon modes ZA, TA, and LA contribute predominantly to the total thermal conductivity (up to 88%), and reducing the size of the material to less than 100 nm could significantly hinder the acoustic phonon transport, thereby greatly reducing the lattice thermal conductivity of buckled arsenene. This information will help to guide the material and device design. The highly anisotropic thermal transport in puckered arsenene (30.7 vs 9.6 W m^{-1} K^{-1}) is attributed to the anisotropy of phonon group velocities as well as the anharmonic bonding and vibrations. As shown in Figure 1 and Figure S4, the phonon group velocity along the ZZ direction is apparently larger than that along the AC direction. Meanwhile, the Grüneisen parameter in the ZZ direction is smaller than that in the AC direction, which indicates less anharmonic lattice vibrations and longer phonon relaxation times in the ZZ direction. The anisotropic bonding and anharmonicity of vibrations in puckered arsenene can also be manifested by the energy variation with the atomic displacement in the ZZ and AC directions, respectively. The energy curve deviates appreciably from that of the harmonic oscillator when the arsenic atom moves in the AC direction (Figure S5).

3.3. Thermoelectric Transport Properties. By shifting the Fermi level in the Fermi−Dirac distribution function, we can mimic the doping process and obtain the electrical

DOI: 10.1021/acs.jpcc.7b06196
J. Phys. Chem. C 2017, 121, 19080−19086

conductivity, the Seebeck coefficient, and the electronic thermal conductivity as a function of the carrier concentration. The electrical transport coefficients of puckered arsenene at 300 K are presented in Figure 4, and those of buckled arsenene are

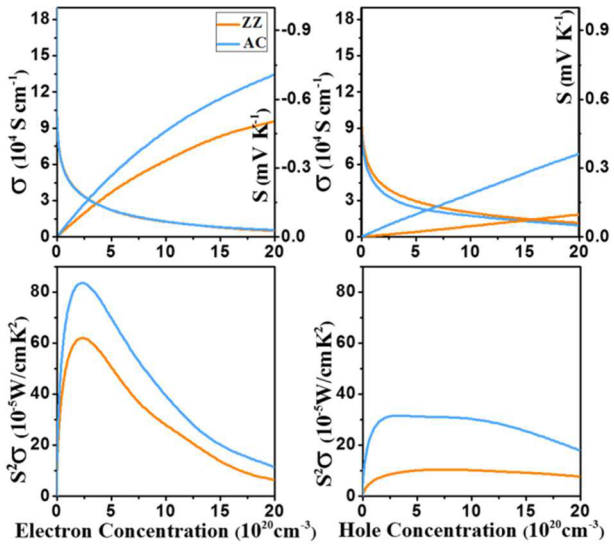

Figure 4. Electrical conductivity σ, Seebeck coefficient S, and power factor $S^2\sigma$ in puckered arsenene as a function of carrier concentration at 300 K.

provided in Figure S6. The Seebeck coefficient is related to the density of states, so it is almost isotropic in puckered arsenene, unlike the mobility and electrical conductivity. The Seebeck coefficient decreases dramatically with the increasing carrier density, indicating that optimizing the carrier density is crucial for achieving efficient thermoelectric performance. In puckered arsenene, the power factor $S^2\sigma$ maximizes at the carrier concentration between 2×10^{20} and 6×10^{20} cm^{-3}. For holes, its peak value along the AC direction is about 3 times larger than that along the ZZ direction, while, for electrons, it is only slightly larger. The electronic thermal conductivity is proportional to the electrical conductivity, usually following the Wiedemann–Franz law $\kappa_e = L\sigma T$ (L is the Lorenz number), and its value is ~4 W m^{-1} K^{-1} at a carrier concentration of 2×10^{20} cm^{-3}, corresponding to $L = 0.7L_0$ ($L_0 = 2.45 \times 10^{-8}$ W Ω K^{-2} is the Sommerfeld theoretical value for free electrons). Therefore, at the optimal doping level, the main contribution to the total thermal conductivity arises from the lattice thermal conductivity, which is 9.6 W m^{-1} K^{-1} in the AC direction and 30.7 W m^{-1} K^{-1} in the ZZ direction as presented above. Figure 5 depicts the room-temperature (300 K) thermoelectric figure of merit ZT = $S^2\sigma T/(\kappa_e + \kappa_L)$ as a function of the carrier concentration in puckered arsenene along the ZZ and AC directions, respectively. Since the preferential directions of electrical and thermal conduction are orthogonal to each other, the maximum value of ZT in puckered arsenene along the AC direction can be as high as 1.6 for electrons and 0.7 for holes at room temperature. Such a phenomenon of orthogonal electrical and thermal transport has also been observed in other group VA elemental materials such as black phosphorene. This unique feature can be attributed to the special puckered structure of group VA 2D materials.[6,49] Due to the orthogonal transport of heat and charge, the ZT value exhibits even larger anisotropy, with that along the AC direction much larger than that along the ZZ direction for both

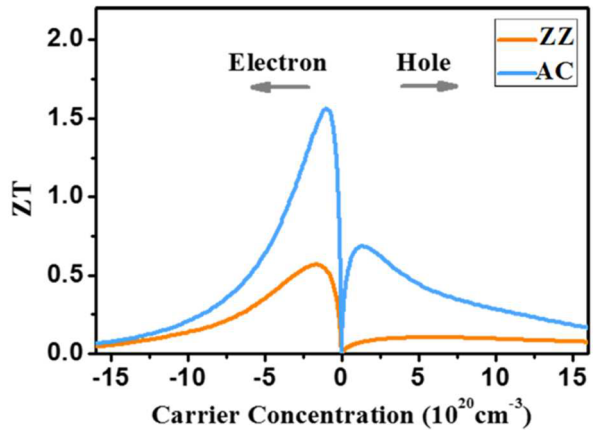

Figure 5. Thermoelectric figure of merit (ZT) of puckered arsenene at 300 K along the zigzag (ZZ) and armchair (AC) directions, respectively.

electrons (1.6 vs 0.6) and holes (0.7 vs 0.1). Significantly, unlike most thermoelectric materials whose thermoelectric figure of merit diminishes at lower temperatures, such as black phosphorene (0.03–0.06),[50] monolayer TMDs (~0.05 for MoS_2, ~0.1 for $MoSe_2$, ~0.2 for WSe_2),[51,52] and monolayer $SnSe_2$ (0.5–0.9),[53] the ZT value of puckered arsenene along the AC direction is substantial at room temperature. This merit makes puckered arsenene a promising candidate for thermoelectric cooling applications. As for the buckled arsenene, due to its relatively high lattice thermal conductivity and relatively small carrier mobility, the ZT values at 300 K are lower than 0.2 for both electrons and holes (Figure S7). We noticed that the high room-temperature ZT of 2.15 was predicted in the buckled antimonene in a recent first-principles study.[54] However, the ballistic charge and phonon transports were investigated there, without taking into consideration the electron–phonon and phonon–phonon interactions. In bulk materials, the transports of charge and phonons are dominated by scattering events. In this work, the electron-acoustic phonon scattering and phonon–phonon scattering are explicitly calculated.

4. CONCLUSIONS

In summary, we have applied the first-principles method and the Boltzmann transport theory to investigate the charge transport, phonon transport, and thermoelectric properties of monolayer arsenic featuring buckled and puckered structures. Unlike their bulk counterparts, both of them are indirect band gap semiconductors with band gaps of 2.07 and 1.36 eV at the HSE06 level of theory. They exhibit moderate to high electron and hole mobilities on the order of 10^2–10^3 cm^2/(V s). More importantly, due to its anharmonic and anisotropic bonding and the heavy atomic mass, puckered arsenene possesses a relatively low lattice thermal conductivity, as compared to graphene, black phosphorene, and other known 2D materials. The poor thermal conduction along the AC direction in puckered arsenene is attributed to its soft vibrations and high Grüneisen parameters which reflect the anharmonicity of bonding. Amazingly, it has also been found that the electrical and thermal conductions exhibit such an anisotropy that their respective preferred directions of conduction are orthogonal to each other, which results in an enhanced thermoelectric figure of merit and an enlarged anisotropy in puckered arsenene. The dimensionless figure of merit at room temperature is as high as

DOI: 10.1021/acs.jpcc.7b06196
J. Phys. Chem. C 2017, 121, 19080–19086

1.6 along the armchair direction when n-doped, which makes puckered arsenene an extremely promising candidate for thermoelectric cooling applications.

■ ASSOCIATED CONTENT

Supporting Information

The Supporting Information is available free of charge on the ACS Publications website at DOI: 10.1021/acs.jpcc.7b06196.

Supplementary figures and tables, computational details, and supplementary references (PDF)

■ AUTHOR INFORMATION

Corresponding Author

*E-mail: dong913@tsinghua.edu.cn.

ORCID

Dong Wang: 0000-0002-0594-0515

Zhigang Shuai: 0000-0003-3867-2331

Notes

The authors declare no competing financial interest.

■ ACKNOWLEDGMENTS

This work is supported by the National Natural Science Foundation of China (Grant Nos. 21673123, 21290190, and 91333202) and the Ministry of Science and Technology of China (Grant Nos. 2015CB655002 and 2013CB933503). Computational resources are provided by the Tsinghua Supercomputing Center.

■ REFERENCES

(1) Zeier, W. G.; Zevalkink, A.; Gibbs, Z. M.; Hautier, G.; Kanatzidis, M. G.; Snyder, G. J. Thinking Like a Chemist: Intuition in Thermoelectric Materials. *Angew. Chem., Int. Ed.* **2016**, *55*, 6826−41.

(2) Zhao, L. D.; Lo, S. H.; Zhang, Y.; Sun, H.; Tan, G.; Uher, C.; Wolverton, C.; Dravid, V. P.; Kanatzidis, M. G. Ultralow Thermal Conductivity and High Thermoelectric Figure of Merit in SnSe Crystals. *Nature* **2014**, *508*, 373−7.

(3) Zhou, G.; Wang, D. Few-Quintuple Bi_2Te_3 Nanofilms as Potential Thermoelectric Materials. *Sci. Rep.* **2015**, *5*, 8099.

(4) Wang, F. Q.; Zhang, S.; Yu, J.; Wang, Q. Thermoelectric Properties of Single-Layered SnSe Sheet. *Nanoscale* **2015**, *7*, 15962−70.

(5) Lee, M. J.; et al. Thermoelectric Materials by Using Two-Dimensional Materials with Negative Correlation between Electrical and Thermal Conductivity. *Nat. Commun.* **2016**, *7*, 12011.

(6) Fei, R.; Faghaninia, A.; Soklaski, R.; Yan, J. A.; Lo, C.; Yang, L. Enhanced Thermoelectric Efficiency via Orthogonal Electrical and Thermal Conductances in Phosphorene. *Nano Lett.* **2014**, *14*, 6393−9.

(7) Chen, J.; Chen, S.; Gao, Y. Anisotropy Enhancement of Thermal Energy Transport in Supported Black Phosphorene. *J. Phys. Chem. Lett.* **2016**, *7*, 2518−23.

(8) Koenig, S. P.; Doganov, R. A.; Schmidt, H.; Castro Neto, A. H.; Özyilmaz, B. Electric Field Effect in Ultrathin Black Phosphorus. *Appl. Phys. Lett.* **2014**, *104*, 103106.

(9) Liu, H.; Neal, A. T.; Zhu, Z.; Luo, Z.; Xu, X.; Tomanek, D.; Ye, P. D. Phosphorene: An Unexplored 2D Semiconductor with a High Hole Mobility. *ACS Nano* **2014**, *8*, 4033−4041.

(10) Xia, F.; Wang, H.; Jia, Y. Rediscovering Black Phosphorus as an Anisotropic Layered Material for Optoelectronics and Electronics. *Nat. Commun.* **2014**, *5*, 4458.

(11) Tran, V.; Soklaski, R.; Liang, Y.; Yang, L. Layer-Controlled Band Gap and Anisotropic Excitons in Few-Layer Black Phosphorus. *Phys. Rev. B: Condens. Matter Mater. Phys.* **2014**, *89*, 235319.

(12) Xu, W.; Zhu, L.; Cai, Y.; Zhang, G.; Li, B. Direction Dependent Thermal Conductivity of Monolayer Phosphorene: Parameterization of Stillinger-Weber Potential and Molecular Dynamics Study. *J. Appl. Phys.* **2015**, *117*, 214308.

(13) Qin, G.; Yan, Q. B.; Qin, Z.; Yue, S. Y.; Hu, M.; Su, G. Anisotropic Intrinsic Lattice Thermal Conductivity of Phosphorene from First Principles. *Phys. Chem. Chem. Phys.* **2015**, *17*, 4854−8.

(14) Wang, Y.; et al. Large Anisotropic Thermal Transport Properties Observed in Bulk Single Crystal Black Phosphorus. *Appl. Phys. Lett.* **2016**, *108*, 092102.

(15) Zhu, Z.; Guan, J.; Tománek, D. Strain-Induced Metal-Semiconductor Transition in Monolayers and Bilayers of Gray Arsenic: A Computational Study. *Phys. Rev. B: Condens. Matter Mater. Phys.* **2015**, *91*, 161404.

(16) Zhang, Z. Y.; Xie, J.; Yang, D.; Wang, Y.; Si, M. S.; Xue, D. Manifestation of Unexpected Semiconducting Properties in Few-Layer Orthorhombic Arsenene. *Appl. Phys. Express* **2015**, *8*, 055201.

(17) Zhang, S.; Xie, M.; Li, F.; Yan, Z.; Li, Y.; Kan, E.; Liu, W.; Chen, Z.; Zeng, H. Semiconducting Group 15 Monolayers:A Broad Range of Band Gaps and High Carrier Mobilities. *Angew. Chem., Int. Ed.* **2016**, *55*, 1666−1669.

(18) Zheng, G.; Jia, Y.; Gao, S.; Ke, S. Comparative Study of Thermal Properties of Group-VA Monolayers with Buckled and Puckered Honeycomb Structures. *Phys. Rev. B: Condens. Matter Mater. Phys.* **2016**, *94*, 155448.

(19) Zhang, S.; Yan, Z.; Li, Y.; Chen, Z.; Zeng, H. Atomically Thin Arsenene and Antimonene: Semimetal-Semiconductor and Indirect-Direct Band-Gap Transitions. *Angew. Chem., Int. Ed.* **2015**, *54*, 3112−5.

(20) Kamal, C.; Ezawa, M. Arsenene: Two-Dimensional Buckled and Puckered Honeycomb Arsenic Systems. *Phys. Rev. B: Condens. Matter Mater. Phys.* **2015**, *91*, 085423.

(21) Carrete, J.; Gallego, L. J.; Mingo, N. Structural Complexity and Phonon Physics in 2D Arsenenes. *J. Phys. Chem. Lett.* **2017**, *8*, 1375−1380.

(22) Tsai, H.; Wang, S.-W.; Hsiao, C.; Chen, C.; Ouyang, H.; Chueh, Y.; Kuo, H.; Liang, J. Direct Synthesis and Practical Bandgap Estimation of Multilayer Arsenene Nanoribbons. *Chem. Mater.* **2016**, *28*, 425−429.

(23) Qiao, J.; Kong, X.; Hu, Z. X.; Yang, F.; Ji, W. High-Mobility Transport Anisotropy and Linear Dichroism in Few-Layer Black Phosphorus. *Nat. Commun.* **2014**, *5*, 4475.

(24) Cai, Y.; Zhang, G.; Zhang, Y. W. Polarity-Reversed Robust Carrier Mobility in Monolayer MoS_2 Nanoribbons. *J. Am. Chem. Soc.* **2014**, *136*, 6269−75.

(25) Kresse, G.; Furthmuller, J. Efficient Iterative Schemes for Ab Initio Total-Energy Calculations Using a Plane-Wave Basis Set. *Phys. Rev. B: Condens. Matter Mater. Phys.* **1996**, *54*, 11169−11186.

(26) Kresse, G.; Furthmiiller, J. Efficiency of Ab-Initio Total Energy Calculations for Metals and Semiconductors Using a Plane-Wave Basis Set. *Comput. Mater. Sci.* **1996**, *6*, 15−50.

(27) Perdew, J. P.; Burke, K.; Ernzerhof, M. Generalized Gradient Approximation Made Simple. *Phys. Rev. Lett.* **1996**, *77*, 3865−3868.

(28) Togo, A.; Oba, F.; Tanaka, I. First-Principles Calculations of the Ferroelastic Transition between Rutile-Type and $CaCl_2$-Type SiO_2 at High Pressures. *Phys. Rev. B: Condens. Matter Mater. Phys.* **2008**, *78*, 134106.

(29) Madsen, G. K. H.; Singh, D. J. Boltztrap. A Code for Calculating Band-Structure Dependent Quantities. *Comput. Phys. Commun.* **2006**, *175*, 67−71.

(30) Bardeen, J.; Shockley, W. Deformation Potentials and Mobilities in Non-Polar Crystals. *Phys. Rev.* **1950**, *80*, 72−80.

(31) Long, M.; Tang, L.; Wang, D.; Wang, L.; Shuai, Z. Theoretical Predictions of Size-Dependent Carrier Mobility and Polarity in Graphene. *J. Am. Chem. Soc.* **2009**, *131*, 17728−17729.

(32) Long, M.; Tang, L.; Wang, D.; Y, L.; Shuai, Z. Electronic Structure and Carrier Mobility in Graphdiyne Sheet and Nanoribbons: Theoretical Predictions. *ACS Nano* **2011**, *5*, 2593−2600.

(33) Xi, J.; Long, M.; Tang, L.; Wang, D.; Shuai, Z. First-Principles Prediction of Charge Mobility in Carbon and Organic Nanomaterials. *Nanoscale* **2012**, *4*, 4348−69.

(34) Morelli, D. T.; Heremans, J. P.; Slack, G. A. Estimation of the Isotope Effect on the Lattice Thermal Conductivity of Group IV and Group III-V Semiconductors. *Phys. Rev. B: Condens. Matter Mater. Phys.* **2002**, *66*, 195304.
(35) Slack, G. A.; Galginaitis, S. Thermal Conductivity and Phonon Scattering by Magnetic Impurities in CdTe. *Phys. Rev.* **1964**, *133*, A253−A268.
(36) Nika, D. L.; Ghosh, S.; Pokatilov, E. P.; Balandin, A. A. Lattice Thermal Conductivity of Graphene Flakes: Comparison with Bulk Graphite. *Appl. Phys. Lett.* **2009**, *94*, 203103.
(37) Cao, J. X.; Yan, X. H.; Xiao, Y.; Ding, J. W. Thermal Conductivity of Zigzag Single-Walled Carbon Nanotubes: Role of the Umklapp Process. *Phys. Rev. B: Condens. Matter Mater. Phys.* **2004**, *69*, 043407.
(38) Zhang, Z. Y.; Cao, H. N.; Zhang, J. C.; Wang, Y. H.; Xue, D. S.; Si, M. S. Orientation and Strain Modulated Electronic Structures in Puckered Arsenene Nanoribbons. *AIP Adv.* **2015**, *5*, 067117.
(39) Wang, Y.; Ding, Y. Electronic Structure and Carrier Mobilities of Arsenene and Antimonene Nanoribbons: A First-Principle Study. *Nanoscale Res. Lett.* **2015**, *10*, 955.
(40) Carrete, J.; Li, W.; Lindsay, L.; Broido, D. A.; Gallego, L. J.; Mingo, N. Physically Founded Phonon Dispersions of Few-Layer Materials and the Case of Borophene. *Mater. Res. Lett.* **2016**, *4*, 204−211.
(41) Ladd, A. J. C.; Moran, B.; Hoover, W. G. Lattice Thermal Conductivity: A Comparison of Molecular Dynamics and Anharmonic Lattice Dynamics. *Phys. Rev. B: Condens. Matter Mater. Phys.* **1986**, *34*, 5058−5064.
(42) Schelling, P. K.; Phillpot, S. R.; Keblinski, P. Comparison of Atomic-Level Simulation Methods for Computing Thermal Conductivity. *Phys. Rev. B: Condens. Matter Mater. Phys.* **2002**, *65*, 144306.
(43) McGaughey, A. J. H.; Kaviany, M. Quantitative Validation of the Boltzmann Transport Equation Phonon Thermal Conductivity Model under the Single-Mode Relaxation Time Approximation. *Phys. Rev. B: Condens. Matter Mater. Phys.* **2004**, *69*, 094303.
(44) He, Y.; Savic, I.; Donadio, D.; Galli, G. Lattice Thermal Conductivity of Semiconducting Bulk Materials: Atomistic Simulations. *Phys. Chem. Chem. Phys.* **2012**, *14*, 16209−22.
(45) Jain, A.; McGaughey, A. J. Strongly Anisotropic in-Plane Thermal Transport in Single-Layer Black Phosphorene. *Sci. Rep.* **2015**, *5*, 8501.
(46) Wang, S.; Wang, W.; Zhao, G. Thermal Transport Properties of Antimonene: An Ab Initio Study. *Phys. Chem. Chem. Phys.* **2016**, *18*, 31217−31222.
(47) Zeraati, M.; Vaez Allaei, S. M.; Abdolhosseini Sarsari, I.; Pourfath, M.; Donadio, D. Highly Anisotropic Thermal Conductivity of Arsenene: An Ab Initio Study. *Phys. Rev. B: Condens. Matter Mater. Phys.* **2016**, *93*, 085424.
(48) Wu, X.; Varshney, V.; Lee, J.; Pang, Y.; Roy, A. K.; Luo, T. How to Characterize Thermal Transport Capability of 2D Materials Fairly? − Sheet Thermal Conductance and the Choice of Thickness. *Chem. Phys. Lett.* **2017**, *669*, 233−237.
(49) Medrano Sandonas, L.; Teich, D.; Gutierrez, R.; Lorenz, T.; Pecchia, A.; Seifert, G.; Cuniberti, G. Anisotropic Thermoelectric Response in Two-Dimensional Puckered Structures. *J. Phys. Chem. C* **2016**, *120*, 18841−18849.
(50) Liao, B.; Zhou, J.; Qiu, B.; Dresselhaus, M. S.; Chen, G. Ab Initio Study of Electron-Phonon Interaction in Phosphorene. *Phys. Rev. B: Condens. Matter Mater. Phys.* **2015**, *91*, 235419.
(51) Jin, Z.; Liao, Q.; Fang, H.; Liu, Z.; Liu, W.; Ding, Z.; Luo, T.; Yang, N. A Revisit to High Thermoelectric Performance of Single-Layer MoS_2. *Sci. Rep.* **2016**, *5*, 18342.
(52) Kumar, S.; Schwingenschlögl, U. Thermoelectric Response of Bulk and Monolayer $MoSe_2$ and WSe_2. *Chem. Mater.* **2015**, *27*, 1278−1284.
(53) Li, G.; Ding, G.; Gao, G. Thermoelectric Properties of $SnSe_2$ Monolayer. *J. Phys.: Condens. Matter* **2017**, *29*, 015001.
(54) Chen, K.; Lyu, S.; Wang, X.; Fu, Y.; Heng, Y.; Mo, D. Excellent Thermoelectric Performance Predicted in Two-Dimensional Buckled Antimonene: A First-Principles Study. *J. Phys. Chem. C* **2017**, *121*, 13035−13042.

DOI: 10.1021/acs.jpcc.7b06196
J. Phys. Chem. C 2017, 121, 19080−19086